High-pressure phase of $LaPO_4$ studied by x-ray diffraction and second harmonic generation

J. Ruiz-Fuertes,[1,2,*] A. Hirsch,[3] A. Friedrich,[4] B. Winkler,[2] L. Bayarjargal,[2] W. Morgenroth,[2] L. Peters,[3] G. Roth,[3] and V. Milman[5]

[1]*Departament de Física Aplicada–ICMUV, Universitat de València, Dr. Moliner 50, 46100 Burjassot, Spain*

[2]*Institut für Geowissenschaften, Goethe-Universität, Altenhöferallee 1, 60438 Frankfurt am Main, Germany*

[3]*Institut für Kristallographie, RWTH Aachen Universität, Templergraben 55, 52062 Aachen, Germany*

[4]*Institut für Anorganische Chemie, Julius-Maximilians-Universität Würzburg, Am Hubland, 97074 Würzburg, Germany*

[5]*Dassault Systèmes BIOVIA, 334 Science Park, Cambridge CB4 0WN, United Kingdom*

(Received 10 May 2016; revised manuscript received 10 August 2016; published 28 October 2016)

The pressure-induced phase transition of monazite-type $LaPO_4$ at ≈26 GPa is studied by single-crystal x-ray diffraction and second harmonic generation (SHG) up to 31 GPa. The structure of the postmonazite phase of $LaPO_4$ has been obtained and it is shown that it corresponds to a post-barite-type structure with an acentric space group $P2_12_12_1$. A strong increase of the SHG signal at the transition confirms that the high-pressure polymorph is noncentrosymmetric. The phase transition involves a significant discontinuous decrease of the unit-cell volume by 6%, which is mainly due to a strong contraction of the a lattice parameter. Enthalpy differences between polymorphs with monazite-, barite-, and post-barite-type structures have been obtained from density-functional-theory-based calculations. They also yield a transition pressure of 21 GPa for the monazite to postbarite phase transition, but indicate that the barite-type phase is significantly more stable, implying that the transition into this phase may be kinetically hindered. As the transition pressure for the monazite-type to post-barite-type structure is reproduced with reasonable accuracy, we predict the corresponding phase-transition pressures of $NdPO_4$ and $GdPO_4$ to be 35 and 45 GPa, respectively.

DOI: 10.1103/PhysRevB.94.134109

I. INTRODUCTION

Monazite-type lanthanum phosphate ($LaPO_4$) with a high refractive index [1], large thermal and chemical stability [2,3], high proton conductivity when doped with Ca or Sr [4,5], and low shear moduli [6], is useful in lasing [7], bioimaging applications [8,9], proton-conducting solid oxide fuel cells [10,11], and interlayer coatings [12,13].

The monazite-type structure (space group $P2_1/n$, $Z = 4$), which is characterized by isolated PO_4 tetrahedra only connected to the large LaO_9 polyhedra as shown in Fig. 1(a), is the ground state structure of the orthophosphates which incorporates light lanthanides (La-Gd), while orthophosphates incorporating a heavy lanthanide ion prefer to crystallize in a xenotime-type structure (space group $I4_1/amd$, $Z = 4$). In the xenotime-type structure the lanthanide ion is eightfold instead of ninefold coordinated.

Several studies have shown that at high pressure, xenotime-type orthophosphates first transform into monazite-type structures, either directly as in YPO_4 [14], or indirectly as in $Tb_{0.5}Gd_{0.5}PO_4$ [15]. Further pressure increase then leads to "postmonazite" phases, with a structure yet unknown. Lacomba-Perales *et al.* [14] reported a phase transition of $LaPO_4$ to an orthorhombic phase at 26 GPa using powder x-ray diffraction (XRD). However, due to strongly overlapping Bragg reflections, they could not solve the structure, but proposed the centrosymmetric barite-type structure (space group *Pnma*) as the most plausible one [14].

The determination of the postmonazite structure would provide insight into the pressure behavior not only of the family of monazite-type orthophosphates but most probably also of the high-pressure behavior of the xenotime-type orthophosphates.

In order to solve the postmonazite phase we have chosen $LaPO_4$ as it has a monazite-type structure already at ambient conditions, and among these orthophosphates it shows the lowest phase-transition pressure, i.e., 26 GPa [14]. Since powder XRD has shown to be an inefficient technique for solving the problem before [14], we employed single-crystal XRD (SXRD). Complementary second harmonic generation (SHG) experiments and *ab initio* calculations have been carried out and are discussed with respect to the high-pressure structure of $LaPO_4$ obtained from single-crystal XRD.

II. EXPERIMENTAL DETAILS

$LaPO_4$ single crystals with diameters in a range of 3–5 mm were grown following the flux method of Cherniak *et al.* [16]. A flux composed of 75 mol % MoO_3 and 25 mol % Li_2CO_3 was mixed with the monazite powder, previously prepared by a solid state reaction at 1523 K [17], in a molar ratio of 100:2 flux:sample. The mixture was heated to 1623 K and kept at this temperature for 15 h to assure complete dissolution and homogenization, then cooled with a ramp of 1–3 K/h to 1143 K. At this temperature the crucibles were removed from the oven. After cooling, the flux material was dissolved in H_2O in an ultrasonic bath. High-pressure experiments were performed using Boehler-Almax diamond-anvil cells (DACs) with diamonds of 350-μm culet sizes [18]. Two (001)-oriented single crystals of $LaPO_4$ with a size of $40 \times 40 \times 10\ \mu m^3$ were loaded in separate DACs in a 130-μm-diam hole in tungsten gaskets preindented to a thickness of 40 μm. Ruby chips were also loaded for pressure determination [19]. Neon was employed as a quasihydrostatic pressure-transmitting medium [20]. The single-crystal XRD experiments were performed at

*javier.ruiz-fuertes@uv.es

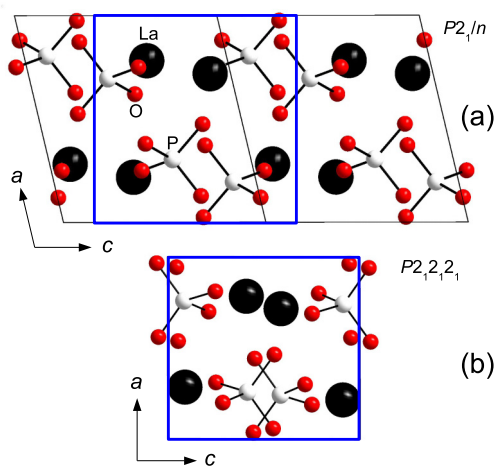

FIG. 1. Projections along the [010] direction of the (a) monazite-type structure and of the (b) post-monazite-type (post-barite-like) structure of $LaPO_4$ as derived from our experiments at 27 GPa. Comparable sections of the crystal structures are highlighted in blue. The large black spheres represent the La atoms and the small white and red spheres represent the P and O atoms, respectively.

the Extreme Conditions Beamline (ECB) at PETRA III ($\lambda = 0.2907$ Å using a Perkin Elmer XRD 1621 flat-panel detector, placed at 451 mm from the sample and a beam focused down to $2.1 \times 2.4\ \mu m^2$ [full width at half maximum (FWHM)]. Six SXRD experiments were carried out at 8.0(1), 12.9(1), 16.7(1), 21.2(1), 27.1(1), and 31.2(2) GPa. The diffraction images were collected by 1° ω scanning over a range of 75° or 66° depending on the DAC used. The image format was converted according to the procedure described by Rothkirch *et al.* [21] for further processing with the CrysAlis^{Pro} software [22] for indexing reflections and intensity data reduction. Crystal structures were first determined using the Patterson method with SHELXS97 and then refined with SHELXL97 [23]. The SHG intensities were measured at $\lambda_{2\omega} = 527$ nm in transmission geometry using the setup described by Bayarjargal *et al.* [24] employing a neodymium-doped yttrium lithium fluoride (Nd:YLF) pulsed laser at $\lambda = 1054$ nm. For the SHG experiments some crystals were ground to fine powders and then compacted into 20-μm-thick pellets. Similarly to the XRD experiments, the pellets were loaded in a 40-μm-thick tungsten gasket and neon was employed as pressure-transmitting medium.

III. *AB INITIO* CALCULATIONS

Ab initio calculations for $LaPO_4$, $NdPO_4$, and $GdPO_4$ in the monazite-, barite-, and post-barite-type structures were carried out at pressures up to 50 GPa. We used a plane-wave pseudopotential approach to density functional theory (DFT) as implemented in the CASTEP package [25]. Spin-polarized calculations were performed with a generalized gradient approximation (GGA) in the Wu-Cohen formulation [26] and ultrasoft-type pseudopotentials from the "on the fly" database of Accelrys Materials Studio 7. The reciprocal space was sampled according to the Monkhorst-Pack scheme [27] with a distance of $\approx 0.035\ Å^{-1}$ between the k points and a plane-wave basis set with a kinetic energy cutoff of 610 eV. We employed a Hubbard U of 6 eV for the f electrons. Variation of the Hubbard U lead to small systematic changes in the structural parameters, but had no significant influence on energy differences.

IV. RESULTS AND DISCUSSION

A. Single-crystal x-ray diffraction

In order to illustrate the evolution of the Bragg reflections with pressure, a section of one single-crystal XRD frame measured at three different pressures is shown in Fig. 2. At 16.7(1) GPa the $(5k\bar{2})$ monoclinic reflections are still sharp, at 21.2(1) GPa start to broaden as a result of the compression, and at 27.1(1) GPa additional reflections appear, indicating the occurrence of the phase transition [Fig. 2(b)].

This phase transition has been observed before at 26.1 GPa with powder XRD at similarly hydrostatic conditions [14]. In that work additional weak reflections were observed above 26.1 GPa and indexed with an orthorhombic metric that the authors proposed to correspond to a barite-type structure. However, given that the low-pressure and high-pressure phases seem to coexist up to the maximum measured pressure (30 GPa) and the small number of additional weak reflections, the structure could not be determined [14]. In our single-crystal XRD experiment at 27.1(1) GPa we observe 1188 reflections from the low-pressure monoclinic phase and 1073 reflections of the high-pressure phase. The absences of reflections can be caused by nonprimitive Bravais lattices or by the presence of translational symmetry elements (screw axes or glide planes). For the high-pressure phase the indexing shows an orthorhombic lattice and the absence of integral reflection conditions. This indicates the absence of lattice centering and hence a primitive lattice (P). Regarding the symmetry elements, in Table I we show the analysis of the zonal and serial reflection conditions that would indicate the presence of translational symmetry elements in each crystallographic direction.

We observe that in the three axes the systematic extinctions are violated for all the glide planes, while the presence of a screw axes in the a and b directions is confirmed. Due to the (001) orientation of the crystal plate within the diamond anvil cell, no (00l) reflections could be measured. Hence, the presence or absence of a screw axis parallel to the c axis cannot be evaluated on the basis of the reflection condition. This reduces the number of possible space groups for the high-pressure structure of $LaPO_4$ to the noncentrosymmetric space groups $P2_12_12_1$ and $P2_12_12$. However, comparing the number of solved structures in both space groups at the ICSD,

TABLE I. Number of observed reflections at 27.1(1) GPa that violate reflection conditions of possible symmetry elements in the three crystallographic directions of the high-pressure structure of $LaPO_4$.

	a				**b**				**c**			
Elements	2_1	b	c	n	2_1	a	c	n	2_1	a	b	n
Absences	8	16	19	19	7	34	36	32	0	114	121	121
Violations	0	12	9	11	0	13	23	24	0	70	97	73

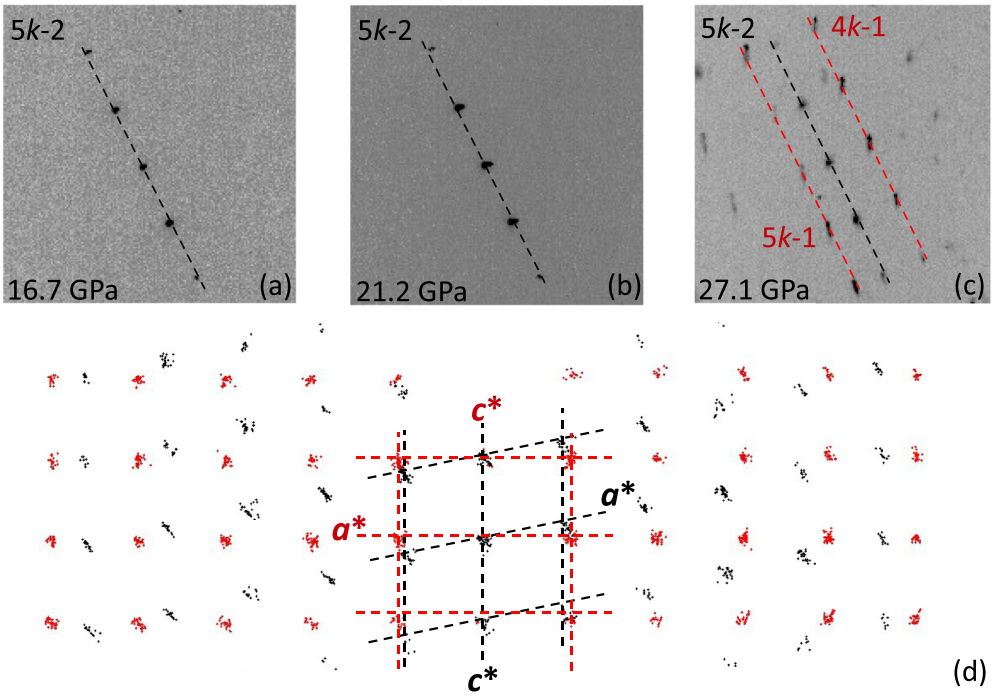

FIG. 2. Section of a SXRD frame of $LaPO_4$ measured at (a) 16.7(1), (b) 21.2(1), and (c) 27.1(1) GPa, showing the evolution of the $5k\bar{2}$ family of reflections. The reflections indexed to the monoclinic phase are labeled in black while the reflection indexes belonging to the high-pressure orthorhombic phase are in red. (d) Corresponding projection of the reciprocal lattice on the (010) plane is shown at 27.1(1) GPa. Dots represent the location of the measured reflections projected along the b^* axis. The unit cells are shown as dashed lines. The monoclinic indexed reflections are in black while the orthorhombic reflections are in red.

the probability of finding a structure with the space group $P2_12_12$ is only 5% of that of $P2_12_12_1$. Finally, the crystal structure could be determined in the space group $P2_12_12_1$. A search for higher symmetry of the obtained crystal structure using the program PLATON [28] did not succeed. This lets us conclude that the space group of the high-pressure phase of $LaPO_4$ is the noncentrosymmetric $P2_12_12_1$. Further evidence supporting a noncentrosymmetric space group is given by the reflection intensity statistics on the basis of the mean $|E^2 - 1|$ value, which closely fits to the ideal value (0.736) of a noncentrosymmetric structure at high probability, and in Sec. IV B.

A projection of the reciprocal space on the (010) plane is shown in Fig. 2(d). It shows the relation between the monoclinic and orthorhombic unit cells.

The atomic coordinates of the high-pressure phase of $LaPO_4$ at 27.1(1) GPa [Fig. 1(b)] are shown in Table II in comparison with the calculated values at 27 GPa. See the Supplemental Material [29] for the refinement results and the structural data of $LaPO_4$ at other pressures. The postmonazite structure retains the P^{5+} ions in fourfold coordination while the coordination of La^{3+} ions changes from nine to 12, similarly to a distorted version of the barite-type structure.

These structural features resemble those of the high-pressure polymorph of barite, $BaSO_4$, [30], which has the same space group $P2_12_12_1$, $Z = 4$. The comparison cannot be direct since our setting has been chosen to be comparable with the monazite-type unit cell and the setting selected by Santamaría-Pérez *et al.* [30] was chosen to be comparable with the barite-type structure. However, if we exchange the a and b axes and make a translational shift according to the space group symmetry, we can find that both are comparable. Hence, the high-pressure polymorphs of barite and orthophosphate monazites crystallize in the same structure type.

From our single-crystal XRD data we have also obtained the pressure dependence of the lattice parameters, unit-cell volume, and La-O bond distances of $LaPO_4$ (Fig. 3). We have fitted the pressure dependence of the unit-cell volume with a third-order Birch-Murnaghan equation of state and obtained a bulk modulus $B_0 = 125(3)$ GPa with a pressure derivative $B_0' = 4.0(1)$. This bulk modulus is in very good agreement with other monazite-type orthophosphates also measured at hydrostatic conditions, such as $CePO_4$ [$B_0 = 122(2)$ GPa] [31] and $BiPO_4$ ($B_0 = 112$ GPa) [32]. It differs significantly from the bulk modulus reported previously for $LaPO_4$ by Lacomba-Perales *et al.* [14] [$B_0 = 144(2)$ GPa, $B_0' = 4.0(2)$], which is 13% larger. Such a difference cannot be attributed to nonhydrostatic conditions since the same pressure-transmitting medium (Ne) was employed in the earlier powder and the current single-crystal XRD experiments, but might be a consequence of intergrain contacts that would limit the effect of pressure on the unit-cell volume.

The evolution of the lattice parameters across the phase transition [Fig. 3(a)] is extremely anisotropic. There is an abrupt collapse of the a lattice parameter which contracts by 6% from 6.4055(17) to 5.9054(13) Å at 27.1(1) GPa while b and c slightly expand (Table II). Under compression, the PO_4 tetrahedra behave as rigid units that barely contract, while the LaO_9 polyhedra account for most of the unit-cell compression [Fig. 3(b)]. However, at the phase transition, the coordination of La increases to 12-fold, while the average La-O distance

TABLE II. Lattice parameters and atomic coordinates of the monazite-type (space group $P2_1/n$) and post-monazite-type (space group $P2_12_12_1$) structures obtained from our single-crystal XRD experiment at 27.1(1) GPa and calculations at 27 GPa. The lattice parameters are in Å and the β angle in degrees.

		Experiment [27.1(1) GPa]		Calculations (27 GPa)	
		Monazite	Postmonazite	Monazite	Postmonazite
	a	6.4055(17)	5.9054(13)	6.2741	5.8378
	b	6.7158(15)	6.6672(14)	6.7205	6.7693
	c	6.182(14)	6.221(13)	6.2832	6.3167
	β	101.70(8)	90	101.02	90
La	x	0.2696(2)	0.5341(2)	0.25907	0.53461
	y	0.16209(19)	0.8802(2)	0.15940	0.91031
	z	0.1178(6)	0.1605(8)	0.12795	0.13328
P	x	0.2966(11)	0.4916(10)	0.29102	0.49264
	y	0.1679(9)	0.8623(9)	0.15940	0.91327
	z	0.626(3)	0.659(3)	0.63777	0.61290
O1	x	0.235(2)	0.438(3)	0.24664	0.44146
	y	0.004(2)	0.695(3)	−0.00568	0.69297
	z	0.450(7)	0.513(11)	0.47475	0.56775
O2	x	0.375(3)	0.551(3)	0.35966	0.53744
	y	0.343(2)	1.046(3)	0.33840	1.05703
	z	0.505(8)	0.517(12)	0.51753	0.56775
O3	x	0.489(3)	0.694(3)	0.47803	0.65900
	y	0.120(2)	0.820(3)	0.11929	0.78688
	z	0.825(8)	0.794(10)	0.81809	0.79297
O4	x	0.115(3)	0.287(3)	0.09892	0.31302
	y	0.216(3)	0.905(3)	0.19837	0.98517
	z	0.752(9)	0.807(10)	0.74481	0.78670

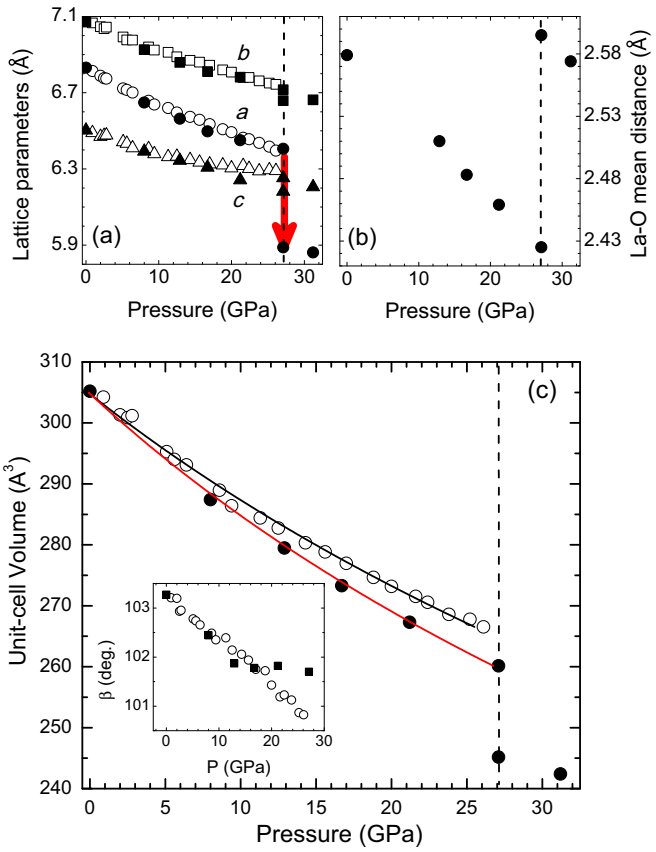

FIG. 3. (a) Lattice parameters of the low- and high-pressure phases of $LaPO_4$. The red arrow indicates the collapse of the a parameter during the phase transition. (b) Pressure dependence of the mean La-O bond distance obtained from our single-crystal XRD experiment. (c) Pressure dependence of the unit-cell volume. The solid symbols are single-crystal XRD data and open symbols are powder XRD data obtained by Lacomba-Perales *et al.* [14]. The continuous red (black) line represents the fit to a third-order Birch-Murnaghan equation of state to the single-crystal (powder) XRD data. The dashed vertical lines indicate the phase transition. The inset shows the pressure dependence of the monoclinic β angle. The errors are smaller than the symbols.

increases abruptly, as the unit-cell volume collapses. This collapse is accommodated by a repacking due to the alignment of the P^{5+} ions in the (100) plane that results in an increase of the overall symmetry.

B. Second harmonic generation

The intensity statistics obtained during the data reduction already indicated that the postmonazite structure probably belongs to a noncentrosymmetric space group, which was strongly supported by the successful structure solution. In order to confirm this finding, we carried out second harmonic generation experiments. SHG, as a nonlinear optical process, is only allowed in systems without inversion symmetry. Its application in high-pressure research has recently been summarized by Bayarjargal and Winkler [33]. The SHG signal can be zero in a noncentrosymmetric space group if the matrix elements of the second-order rank susceptibility tensor are small. However, the detection of a SHG signal that is due to the conversion in the bulk of the sample (in contrast to SHG due to surface effects or due to other defects) unambiguously excludes centrosymmetry.

In Fig. 4 we show the pressure dependence of the intensity of the transmitted light at $\lambda_{2\omega} = 527$ nm of a finely ground $LaPO_4$ powder when excited with a pulsed laser at $\lambda =$ 1054 nm. As long as $LaPO_4$ remains in the centrosymmetric monazite-type structure the SHG signal is absent, but as soon as the phase transition starts (at ∼26 GPa) the SHG signal appears and strongly increases in intensity up to around 29 GPa when the phase-transition process is finished. The signal remains strong up to the maximum measured pressure of 40 GPa. In order to confirm that the SHG signal originates from the bulk, and that a contribution from the grain surfaces is minimal, we have measured the SHG signal at 29.2(1) GPa as a function of the laser current, which is proportional to the laser power. We clearly obtain a quadratic dependence of the SHG signal on the laser power as we show in the inset of Fig. 4, which is typical for SHG in the bulk [33]. This finding confirms that the origin of the SHG signal in $LaPO_4$ above 26 GPa is due to a phase transition from a centrosymmetric space group to a noncentrosymmetric space group, in full agreement with the results of the analysis of the intensity distribution and the structural solution of our single-crystal XRD experiments.

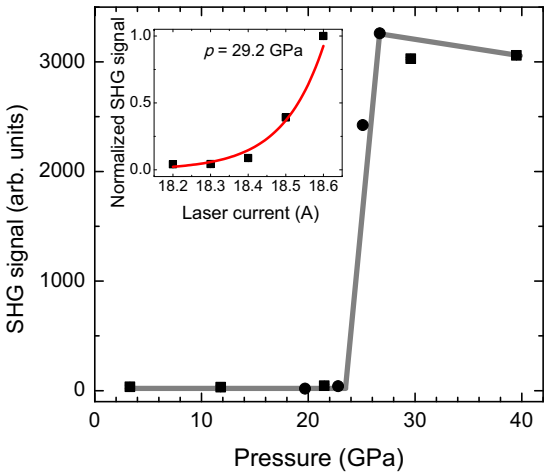

FIG. 4. Pressure dependence of the second harmonic generation (SHG) signal of $LaPO_4$. The inset shows the quadratic dependence of the relative SHG signal at 29.2 GPa with the laser current. In this range the laser current should be directly proportional to the laser power. Different symbols represent different measurements. The gray and red lines are guides to the eye.

C. Calculated phase stability

As we have shown that the postmonazite structure resembles that of the postbarite structure [30] instead of the barite one, as suggested by Lacomba-Perales *et al.* [14], we have carried out *ab initio* calculations for $LaPO_4$ polymorphs having the monazite, barite, or postbarite structure. In the case of the postbarite polymorph we have used the structure obtained from our single-crystal XRD study as a starting model. The calculated enthalpy differences with respect to the monazite-type structure are shown in Fig. 5.

We have found that the post-barite-type structure becomes more stable above 21 GPa, in reasonably good agreement with our experimental results (26 GPa) which are consistent with a previous study [14]. However, the calculations suggest that the barite-type structure is more stable than the other two polymorphs above 10 GPa. The computed enthalpy differences are significant. It is very unlikely that free-energy calculations would change the result, as there is no substantial change in the interatomic interactions, and hence the phonon densities of state will be similar. This indicates that a large kinetic barrier must be hindering this phase transition. These findings are similar to those for $BiPO_4$, where calculations [32] predict a phase transition to a monazite-type structure at 15 GPa while experimentally no phase transition is observed up to 30 GPa. Whether a kinetic barrier is present can be investigated by high-temperature, high-pressure experiments, and such experiments are currently being planned.

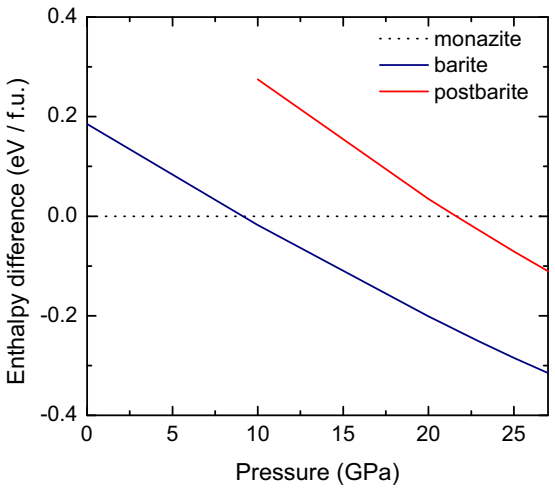

FIG. 5. Calculated enthalpy difference of barite and post-barite-type polymorphs of $LaPO_4$ with respect to the enthalpy of the low-pressure monazite-type one.

In Table II we have shown that the calculations on $LaPO_4$ give lattice parameters which are in very good agreement (to within 2% for the monazite-type phase and to within 3% for the polymorph with the postbarite structure) with our experimental results. The atomic coordinates obtained from the DFT calculations agree well for both monazite- and post-monazite-type phases. The computed bulk modulus $B_{0,\mathrm{theo}} = 111.5(8)$ GPa for monazite-type $LaPO_4$ is 10% smaller than the experimental value obtained in the present single-crystal XRD experiment. This is typical for DFT-GGA calculations [34]. Our value is 10% larger than the value calculated previously by Wang *et al.* [6]. However, as in the latter study no Hubbard U was employed, another GGA was used, and the bulk modulus was obtained from finite strain calculations, a better agreement cannot be expected.

Since the post-barite-type structure probably is representative for all lanthanide orthophosphate monazites, we have calculated the phase stability of the monazite-type and post-barite-type polymorphs of $NdPO_4$ and $GdPO_4$. Our calculations indicate that these compounds would also undergo a phase transition to a post-barite-type structure. The relative stabilities of $NdPO_4$ and $GdPO_4$ at high pressures are similar

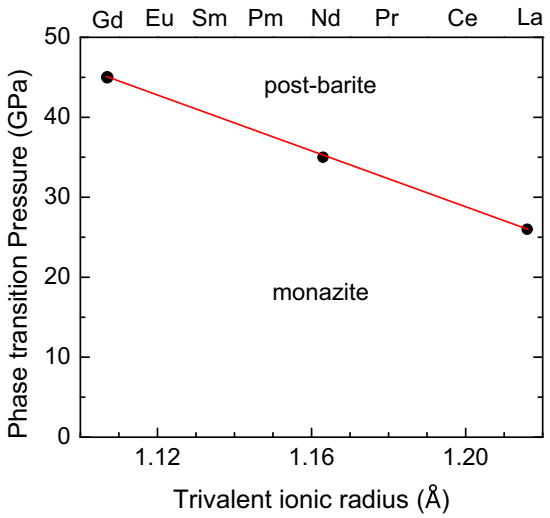

FIG. 6. Calculated phase-transition pressures for $LaPO_4$, $NdPO_4$, and $GdPO_4$ assuming a monazite to postbarite phase transition in the whole family of monazites. Plotting this as a function of the ionic radius of the trivalent cations serves to estimate the expected phase-transition pressure for the whole family.

to those of $LaPO_4$ described above, i.e., in the athermal limit at high pressures the barite-type structure is more stable than the post-barite-type structure, and here as well, high-pressure, high-temperature experiments are required to establish if the transition into the barite-type structure is kinetically hindered.

The results are shown in Fig. 6 where the calculated phase-transition pressures (P_T) are plotted as a function of the ionic radius of the trivalent lanthanide ions in ninefold coordination [35]. With transition pressures P_T of 35 and 45 GPa for $NdPO_4$ and $GdPO_4$, respectively, and a value of $P_T = 21$ GPa for $LaPO_4$, the transition pressure seems to be linearly correlated to the ionic radius of the lanthanide ion.

V. CONCLUDING REMARKS

The high-pressure phase of $LaPO_4$ has been obtained at 27.1(1) GPa using single-crystal x-ray diffraction (XRD). It has been found that the postmonazite structure is similar to the post-barite-type structure [30] observed in $BaSO_4$ at high pressure and not to the barite-type structure previously proposed [14]. The structure is described in the noncentrosymmetric space group $P2_12_12_1$. The absence of inversion symmetry is confirmed by our second harmonic generation study. *Ab initio* calculations performed for $LaPO_4$, $NdPO_4$, and $GdPO_4$ predict the structural phase transition from the monazite- to the post-barite-type structure at 21, 35, and 45 GPa, respectively. However, the calculations also predict at lower pressures a phase transition to the barite-type structure in the three compounds, experimentally not observed in $LaPO_4$. This indicates the existence of a large kinetic barrier between the monazite- and the barite-type phases that might be overcome at high temperatures. Currently, high-pressure and high-temperature experiments in $LaPO_4$ are planned to explore this hypothesis. The higher compressibility found in the monazite-type phase of $LaPO_4$ by our single-crystal XRD experiment with a bulk modulus 13% smaller than that obtained in a powder XRD experiment [14] suggests the existence of deviatoric stresses above 10 GPa caused by intergrain contacts in the powder XRD experiment.

ACKNOWLEDGMENTS

J.R.-F. thanks the Alexander von Humboldt Foundation for a postdoctoral fellowship and the Spanish MINECO for the Juan de la Cierva program (IJCI-2014-20513). B.W. and W.M. acknowledge financial support from the BMBF (05K13RF1). A.H. thanks the BMBF (02NUK021E) for funding. DESY Photon Science is gratefully acknowledged. PETRA III at DESY is a member of the Helmholtz Association (HGF).

[1] P. Ghosh, J. Oliva, E. de la Rosa, K. K. Haldar, D. Solis, and A. Patra, J. Phys. Chem. C **21**, 203 (2001).
[2] W. van Schaik, S. H. M. Poort, G. Blasse, J. A. Pérez-Omil, and S. Bernal-Márquez, Chem. Mater. **6**, 755 (1994).
[3] D. M. Pimpalshende and S. J. Dhoble, Luminescence **144**, 30 (2015).
[4] T. Norby and N. Christiansen, Solid State Ionics **77**, 240 (1995).
[5] K. Amezawa, H. Maekawa, Y. Tomii, and N. Yamamoto, Solid State Ionics **145**, 233 (2001).
[6] J. Wang, Y. Zhou, and Z. Lin, Appl. Phys. Lett. **87**, 051902 (2005).
[7] E. Nakawaza and F. Shiga, Jpn. J. Appl. Phys. **42**, 1642 (2003).
[8] D. K. Chatterjee, A. J. Rufaihah, and Y. Zhang, Biomaterials **29**, 937 (2008).
[9] F. T. Rabouw, S. A. den Hartog, T. Senden, and A. Meijerink, Nat. Commun. **5**, 3610 (2014).
[10] S. M. Haile, D. A. Boysen, C. R. I. Chisholm, and R. B. Merle, Nature (London) **410**, 910 (2001).
[11] S. Phadke, J. C. Ninob, and M. S. Islam, J. Mater. Chem. **22**, 25388 (2012).
[12] P. E. D. Morgan and D. B. Marshal, J. Am. Ceram. Soc. **78**, 1553 (1995).
[13] R. S. Hay, Ceram. Ceram. Eng. Sci. Proc. **21**, 203 (2001).
[14] R. Lacomba-Perales, D. Errandonea, Y. Meng, and M. Bettinelli, Phys. Rev. B **81**, 064113 (2010).
[15] O. Tschauner, S. V. Ushakov, A. Navrotsky, and L. A. Boatner, J. Phys.: Condens. Matter **28**, 035403 (2016).
[16] D. Cherniak, J. Pyle, and J. Rakovan, Am. Mineral. **89**, 1533 (2004).
[17] D. Bregiroux, O. Terra, F. Audubert, N. Dacheux, V. Serin, and R. Podor, Inorg. Chem. **46**, 10372 (2007).
[18] R. Boehler, Rev. Sci. Instrum. **77**, 115103 (2006).
[19] H. K. Mao, J. Xu, and P. M. Bell, J. Geophys. Res. **91**, 4673 (1986).
[20] S. Klotz, J.-C. Chervin, P. Munsch, and G. L. Marchand, J. Phys. D: Appl. Phys. **42**, 075413 (2009).
[21] A. Rothkirch, G. D. Gatta, M. Meyer, S. Merkel, M. Merlini, and H. P. Liermann, J. Synchrotron Radiat. **20**, 711 (2013).
[22] Agilent, Crysalis^{Pro} software system, version 1.171.36.28, Agilent Technologies UK Ltd., Oxford, U.K., 2013.
[23] G. M. Scheldrick, Acta Crystallogr. A **64**, 112 (2008).
[24] L. Bayarjargal, B. Winkler, E. Haussühl, and R. Boehler, Appl. Phys. Lett. **95**, 061907 (2009).
[25] S. J. Clark, M. D. Segall, C. J. Pickard, P. J. Hasnip, M. J. Probert, K. Refson, and M. C. Paynei, Z. Kristallogr. **220**, 567 (2005).
[26] Z. G. Wu and R. E. Cohen, Phys. Rev. B **73**, 235116 (2006).
[27] H. J. Monkhorst and J. D. Pack, Phys. Rev. B **13**, 5188 (1976).
[28] A. L. Spek, J. Appl. Crystallogr. **36**, 7 (2003).
[29] See Supplemental Material at http://link.aps.org/supplemental/10.1103/PhysRevB.94.134109 for structural refinement results and structural data of $LaPO_4$ from 16.7(1) to 31.2(2) GPa.
[30] D. Santamaría-Pérez, L. Gracia, G. Garbarino, A. Beltrán, R. Chuliá-Jordán, O. Gomis, D. Errandonea, C. Ferrer-Roca, D. Martínez-García, and A. Segura, Phys. Rev. B **84**, 054102 (2011).
[31] T. Huang, J. S. Lee, J. Kung, and C.-M. Lin, Solid State Commun. **150**, 1845 (2010).
[32] D. Errandonea, O. Gomis, D. Santamaría-Pérez, B. García-Domene, A. Muñoz, P. Rodríguez-Hernández, S. N. Achary, A. K. Tyagi, and C. Popescu, J. Appl. Phys. **117**, 105902 (2015).
[33] L. Bayarjargal and B. Winkler, Z. Kristallogr. **229**, 92 (2014).
[34] B. Winkler and V. Milman, Z. Kristallogr. **112**, 112 (2014).
[35] R. D. Shannon, Acta Crystallogr. A **32**, 751 (1976).